Multiomic profiling of transplant glomerulopathy reveals a novel T-cell dominant subclass

OPEN

Iacopo Cristoferi[1,2,9], Hilal Varol[1,9], Myrthe van Baardwijk[1,2], Layla Rahiem[1], Karishma A. Lila[1], Thierry P.P. van den Bosch[1], Carla C. Baan[3], Dennis A. Hesselink[3], Rafael Kramann[3,4,5], Robert C. Minnee[2], Dana A.M. Mustafa[6], Marlies E.J. Reinders[3], Dave L. Roelen[7], Shazia P. Shahzad-Arshad[1], Rex N. Smith[8], Andrew P. Stubbs[1], Robert B. Colvin[8], Ivy A. Rosales[8] and Marian C. Clahsen-van Groningen[1,4]

[1]Department of Pathology and Clinical Bioinformatics, Erasmus MC Transplant Institute, Rotterdam, the Netherlands; [2]Department of Surgery, Division of HPB & Transplant Surgery, Erasmus MC Transplant Institute, Rotterdam, the Netherlands; [3]Department of Internal Medicine, Division of Nephrology and Transplantation, Erasmus MC Transplant Institute, Rotterdam, the Netherlands; [4]Institute of Experimental Medicine and Systems Biology, RWTH Aachen University, Aachen, Germany; [5]Department of Nephrology and Clinical Immunology, University Hospital Aachen, RWTH Aachen University, Aachen, Germany; [6]Department of Pathology and Clinical Bioinformatics, the Tumor Immuno-Pathology Laboratory, Erasmus MC Transplant Institute, Rotterdam, the Netherlands; [7]Department of Immunology, Leiden University Medical Center, Leiden, the Netherlands; and [8]Department of Pathology, Massachusetts General Hospital, Harvard Medical School, Boston, Massachusetts, USA

Kidney transplant (KTx) biopsies showing transplant glomerulopathy (TG) (glomerular basement membrane double contours (cg) > 0) and microvascular inflammation (MVI) in the absence of C4d staining and donor-specific antibodies (DSAs) do not fulfill the criteria for chronic active antibody–mediated rejection (CA-AMR) diagnosis and do not fit into any other Banff category. To investigate this, we initiated a multicenter intercontinental study encompassing 36 cases, comparing the immunomic and transcriptomic profiles of 14 KTx biopsies classified as cg + MVI DSA$^-$/C4d$^-$ with 22 classified as CA-AMR DSA$^+$/C4d$^+$ through novel transcriptomic analysis using the NanoString Banff-Human Organ Transplant (B-HOT) panel and subsequent orthogonal subset analysis using two innovative 5-marker multiplex immunofluorescent panels. Nineteen genes were differentially expressed between the two study groups. Samples diagnosed with CA-AMR DSA$^+$/C4d$^+$ showed a higher glomerular abundance of natural killer cells and higher transcriptomic cell type scores for macrophages in an environment characterized by increased expression of complement-related genes (i.e., C5AR1) and higher activity of angiogenesis, interstitial fibrosis tubular atrophy, CA-AMR, and DSA-related pathways when compared to samples diagnosed with cg + MVI DSA$^-$/C4d$^-$. Samples diagnosed with cg + MVI DSA$^-$/C4d$^-$ displayed a higher glomerular abundance and activity of T cells (CD3$^+$, CD3$^+$CD8$^+$, and CD3$^+$CD8$^-$). Thus, we show that using novel multiomic techniques, KTx biopsies with cg + MVI DSA$^-$/C4d$^-$ have a prominent T-cell presence and activity, putting forward the possibility that these represent a more T-cell dominant phenotype.

Kidney International (2024) ■, ■–■; https://doi.org/10.1016/j.kint.2023.11.026

KEYWORDS: chronic rejection; immunohistochemistry; kidney transplantation; transcriptomics; transplant glomerulopathy

Lay Summary

In this study, we compared 2 kidney transplant biopsy rejection diagnoses: one with a rejection type called "chronic-active antibody-mediated rejection" and another that under the microscope looks the same but does not have all the criteria for that diagnosis. Using new and state-of-the-art techniques, we found distinct differences in the biological characteristics between the 2 groups, suggesting that the second group is a different type of rejection with a high presence of T cells. The study will help improve how to diagnose and treat kidney transplant patients with this type of chronic rejection.

The development of chronic-active antibody-mediated rejection (CA-AMR) in kidney transplants (KTxs) represents an intermediate stage in the progression of morphologic lesions from active to chronic AMR and has a large impact on long-term transplant outcome.[1–4] According to the Banff Classification of Allograft Pathology 2019 update,[5] CA-AMR can be diagnosed when 3 diagnostic criteria are met: (i) the presence of morphologic evidence of chronic tissue injury, for example, transplant glomerulopathy (TG, *cg* >0); (ii) evidence of current/recent antibody interaction with vascular endothelium, for example, microvascular inflammation (MVI); and (iii) serologic evidence of circulating donor-specific antibodies (DSAs to human leukocyte antigen [HLA]

Correspondence: *Iacopo Cristoferi or Marian C. Clahsen-van Groningen, Department of Pathology and Clinical Bioinformatics, Erasmus MC Transplant Institute, Room Ee-1579, PO Box 2040, 3000 CA Rotterdam, the Netherlands. E-mail: i.cristoferi@erasmusmc.nl or m.clahsen-vangroningen@erasmusmc.nl*

[9]IC and HV share first authorship.

Received 13 June 2023; revised 4 September 2023; accepted 16 November 2023

or other antigens) that can be substituted by C4d staining of peritubular capillaries (ptcs) (also diagnostic criterion 2) or the presence of validated gene transcripts/classifiers.

Diagnosing CA-AMR remains difficult for several reasons. First, the absence of DSAs at the time of for-cause KTx biopsies does not exclude the presence of CA-AMR. Current antibody testing methods focus on circulating anti-HLA antibodies, thereby missing non-HLA antibodies and possibly leading to false negatives.[6–12] Even when using highly sensitive antibody-detection techniques, in approximately 40% of patients with AMR, no DSAs are detected.[13] Second, C4d scoring is affected by subjectivity,[14] and lack of C4d staining of ptcs is also relatively common in CA-AMR,[15,16] suggesting that TG could occur in the absence of complement activation. Lastly, although promising developments are made in transcriptomic analysis of for-cause kidney biopsies with DSA-selective transcripts,[17] it is not commonly used in clinical practice. Therefore, clinicians identify patients fulfilling only the first 2 diagnostic criteria for the CA-AMR diagnosis showing TG and MVI, testing negative for circulating DSAs with no C4d staining of ptcs, but lacking the opportunity of performing transcript analysis. Hence, there is an unmet need to correctly classify those cases with *cg*+MVI that do not have C4d positivity and DSAs.

To improve classification and therapeutic management, comparison of *cg*+MVI DSA$^-$/C4d$^-$ samples with CA-AMR DSA$^+$/C4d$^+$ samples is needed. Clinical centers encountering *cg*+MVI DSA$^-$/C4d$^-$ patients are usually not able to perform molecular assessments and therefore cannot properly classify their patients within one of the current Banff categories. These cases are often deemed as "histologically comparable to CA-AMR," initiating the same therapeutic strategy as cases fulfilling Banff category 2, CA-AMR. Discussions during the most recent Banff meeting (September 2022 in Banff, Canada) have additionally emphasized the need to not classify those cases as AMR if they do not meet all criteria.[18] *cg*+MVI DSA$^-$/C4d$^-$ samples should be diagnosed as "HLA-DSA-neg MVI cause unclear." It has previously been shown that DSA+ active AMR (A-AMR) cases displayed similar gene expression profiles to cases meeting only the first 2 diagnostic criteria for the AMR diagnosis (MVI) in the absence of DSAs.[19] Multiomic profiling comparing *cg*+MVI DSA$^-$/C4d$^-$ with CA-AMR DSA$^+$/C4d$^+$ cases could render a better understanding of these chronic conditions to improve the current classification and subsequently tailor the therapeutic management.

In this multicenter intercontinental study, we compared the molecular profiles of for-cause KTx biopsies classified as CA-AMR DSA$^+$/C4d$^+$ with those classified as *cg*+MVI DSA$^-$/C4d$^-$ using the comprehensive Banff Human Organ Transplant panel with the innovative NanoString nCounter technology. Afterward, we cross-checked our results on a subset of the cohort through orthogonal analyses including a state-of-the-art multiplex immunofluorescence (mIF) protein analysis using 2 panels focused on the cell types highlighted by our gene expression analysis.

MATERIALS AND METHODS

An extensive description of Materials and Methods is provided in the Supplementary Methods.

Study population

This retrospective multicenter intercontinental study included a highly selected population of KTx recipients. KTx biopsy samples were retrieved from the archives of the Department of Pathology, Erasmus MC, Rotterdam, the Netherlands (Erasmus MC cases, n = 19) and the Department of Pathology, Massachusetts General Hospital, Boston, Massachusetts, USA (Massachusetts General Hospital cases, n = 17). Coherently with the purpose of this study, samples were selected for inclusion if diagnosed with the conditions of interest (including DSA assessment) and if sufficient sample material was available for analysis. Thirty-six transplant recipients who fulfilled the first 2 diagnostic criteria for CA-AMR were retrospectively included in this study (n = 36). Twenty-two patients were classified as CA-AMR DSA$^+$/C4d$^+$, as they had positive C4d staining of ptcs (Banff *C4d* lesion score ≥1) and showed circulating DSAs. The remaining 14 patients were classified as *cg*+MVI DSA$^-$/C4d$^-$ as they did not show C4d-positive staining of ptcs (Banff C4d lesion score = 0) and had no circulating DSAs. Alternative diagnoses compatible with the histomorphologic findings characterizing TG and MVI (and therefore CA-AMR) were excluded[20,21] through the use of clinical information, immunofluorescence, and electron microscopy. The details of the Massachusetts General Hospital cases are presented in a previous report.[22]

Histologic assessment and DSA testing

Formalin-fixed paraffin-embedded specimens were re-evaluated using the 2019 Banff Classification of Allograft Pathology by 2 experienced nephropathologists (IAR and MCC-vG) blinded to the study group the cases belonged to.

Circulating donor-specific anti-HLA DSA assessment was performed with the LIFECODES Donor Specific Antibody Assay (Immucor) using bead-specific cutoffs in combination with a raw mean fluorescence intensity of more than 750 arbitrary units. Data were successively analyzed using MATCH IT! Antibody Analysis Software version 1.3.1 (Immucor).

Survival analysis

The relationship between the diagnosis group and the occurrence of graft failure was investigated through Cox proportional hazards regression adjusted for donor type. Graft survival data were available for the Erasmus MC cases. Details about antirejection therapeutic management of these cases were included in the demographic analysis. Proportional hazards and log-linearity assumptions were verified through the use of Schoenfeld and Martingale residuals, respectively. An additional Kaplan-Meier analysis was performed for visualization purposes.

Gene expression analysis

Gene expression profiles of 35 KTx biopsies (n = 21 CA-AMR DSA$^+$/C4d$^+$ and n = 14 *cg*+MVI DSA$^-$/C4d$^-$) were compared after one initially included sample did not render sufficient amount of RNA for further analysis. The Banff Human Organ Transplant panel using NanoString nCounter technology was used to target the most relevant genes associated with transplant damage.[23] The details of the sample preparation and gene expression analysis of the Massachusetts General Hospital cases were presented in a previous report.[22]

RNA extraction. Details concerning the Erasmus MC cases RNA extraction are provided in the Supplementary Methods.

NanoString nCounter gene expression analysis. Gene expression profiles of the Erasmus MC cases were generated by using the Banff Human Organ Transplant panel within the nCounter FLEX Analysis System (NanoString Technologies, Inc.) following manufacturer's instructions. A total of 490 fields of view were scanned to count the number of copies of each gene in each sample.

mIF analysis

mIF protein orthogonal analysis was performed on the Erasmus MC cases (n = 9 CA-AMR $DSA^+/C4d^+$ and n = 10 *cg*+MVI $DSA^-/C4d^-$) to cross-check results from gene expression analysis.

Immunofluorescence staining panels. Two 5-plex mIF panels feasible on formalin-fixed paraffin-embedded material were custom-developed to investigate the immune cell repertoire in KTx biopsies. Panel 1 is a broad transplantation inflammatory panel using the markers CD3 (pan T cells), CD8 (cytotoxic T cells), CD68 (macrophages), CD31 (endothelial cells), and C4d. Panel 2 focuses on macrophages and monocytes using CD68 (macrophages), CD163 (M2 macrophages), CD14 (M2 macrophages), CD16 (monocytes), and CD56 (natural killer cells). These 2 panels were performed using automated mIF on the BenchMark ULTRA System (Ventana Medical Systems–F. Hoffmann-La Roche AG). An overview of the products and antibodies used for the mIF panels is presented in Supplementary Table S1. A more detailed description of the methodology used for the mIF analysis is provided in the Supplementary Methods.

Multiplex image analysis. All mIF slides were scanned at ×20 magnification using an Axio lmager 2 Fluorescence color microscope (ZEISS). Biopsy samples were analyzed using QuPath Quantitative Pathology & Bioimage Analysis software (version 0.3.0), an open software platform for bioimage analysis.[24] Biopsies were annotated manually to include only cortical tissue and perform compartmental analysis. Using the simple thresholding method, an individual classifier was made for each marker so that the absolute number of cells could be assessed. The data measurements were then exported for further statistical analysis.

Tissue fibrosis assessment

To assess the amount of interstitial fibrosis, Sirius Red staining was performed on the same slides used for mIF panel 2. Slides were scanned using a NanoZoomer 2.0-HT digital slide scanner (Hamamatsu Photonics K.K.) with high resolution (×40). Using QuPath, a training image was created as previously described, and the simple thresholding method was then applied to quantify fibrosis. Medulla, glomeruli, and large blood vessels were manually excluded.

Statistical analysis

Quantitative outcomes and variables (i.e., estimated glomerular filtration rate and Banff scores) were handled as continuous variables. Missing data were excluded from analyses. Cell counts differing from the specific per cell type median value of more than 3 times the per cell type median absolute deviation were labeled as outliers and removed from the analysis. To compare 2 unmatched groups, the Student *t* test was performed after verifying normal distribution. When data were not normally distributed, the Mann-Whitney *U* test was performed. For this study, we considered *P* values and Benjiamini-Hochberg–adjusted *P* values (*q* values) lower than 0.05 to be statistically significant. Unless noted otherwise, results are expressed as mean ± SEM.

Gene expression data analysis. Gene expression data of all the included cases were imported within the R environment for further analysis. Quality control and normalization were performed according to Bhattacharya *et al.*[25] Hierarchical clustering was used to generate heatmaps for additional quality control. Differential expression analysis was performed using *DESeq2*.[26] The Benjamini-Hochberg method was used to adjust the *P* values for multiple testing.[27] The 15 differentially expressed genes with the lowest *q* values were selected to perform a principal component analysis. Successively, gene-set analyses for cell types and pathway scores were performed using renal allograft pathology–specific custom pathway definitions as previously described[22] and generally applicable gene-set enrichment for pathway analysis (*GAGE*).[28]

RESULTS

Study population and demographics

Thirty-six patients were included in this study, with 22 diagnosed with CA-AMR $DSA^+/C4d^+$ and 14 with *cg*+MVI $DSA^-/C4d^-$. No significant difference was found in demographics and antirejection management between the 2 study groups as presented in Table 1.

Histologic assessment

After re-evaluation using the Banff 2019 classification, 5 samples in the CA-AMR $DSA^+/C4d^+$ group also fulfilled the criteria for borderline (suspicious) acute T cell–mediated rejection. However, the 2 study groups were comparable concerning all the individual Banff lesion scores, including interstitial inflammation (*i*), tubulitis (*t*), total inflammation (*ti*), glomerulitis (*g*), and peritubular capillaritis (*ptc*) (Supplementary Table S2).

Survival analysis

Data concerning graft failure, donor type, and antirejection therapy were available only for the Erasmus MC cases. Graft failure occurred in 7 and 3 patients within the CA-AMR $DSA^+/C4d^+$ and *cg*+MVI $DSA^-/C4d^-$ groups, respectively. When performing Cox proportional hazards regression, patients diagnosed with CA-AMR $DSA^+/C4d^+$ showed a higher risk of graft failure occurrence when compared with patients diagnosed with *cg*+MVI $DSA^-/C4d^-$ (hazard ratio = 8.7, confidence interval: 1.1–68.7; $P = 0.040$) after adjusting by donor type (Figure 1).

Gene expression analysis

Sufficient RNA was successfully isolated from 35 samples (n = 21 CA-AMR $DSA^+/C4d^+$ and n = 14 *cg*+MVI $DSA^-/C4d^-$), while 1 sample was excluded because of insufficient amount of material. The significant differentially expressed genes are reported in Table 2. The full list of differential gene expression analysis is presented in Supplementary Table S3. A volcano plot representing the retrieved differential expression analysis data is presented in Figure 2. Nineteen genes were differentially expressed when comparing the 2 study groups. Ten genes displayed higher expression in samples diagnosed with CA-AMR $DSA^+/C4d^+$ compared with samples diagnosed with *cg*+MVI $DSA^-/C4d^-$, including the complement and

Table 1 | Demographics and clinical characteristics of the included study population

Full dataset	CA-AMR DSA$^+$/C4d$^+$ (n = 22)	*cg*+MVI DSA$^-$/C4d$^-$ (n = 14)	*P* value
Recipient			
Sex (female/male)	8/14	4/10	0.90
Age, yr	43.1 ± 18.6 (2.7; 79.5)	49.7 ± 16.8 (15.5; 80.5)	0.23
Time after transplantation, yr	6.4 ± 7.9 (0.2; 31.0)	4.6 ± 3.4 (1.0; 11.2)	0.96
Creatinine at biopsy, mg/dl	2.32 ± 1.03 (0.81; 5.29)	1.85 ± 0.82 (1.01; 4.00)	0.12
Creatinine at 3 yr, mg/dl	4.48 ± 3.35 (0.89; 11.5)	2.10 ± 1.01 (1.29; 4.31)	0.14
Erasmus MC subset	**CA-AMR DSA$^+$/C4d$^+$ (n = 9)**	***cg*+MVI DSA$^-$/C4d$^-$ (n = 10)**	***P* value**
Treatment			
i.v. Ig	9/0	10/0	1.00
Methylprednisolone	9/0	10/0	1.00
Alemtuzumab	8/1	6/4	0.36
Tocilizumab	5/4	1/9	0.10

CA-AMR, chronic-active antibody-mediated rejection; *cg*, Banff glomerular basement membrane double contours lesion score; DSA, circulating donor-specific antibodies; i.v. Ig, intravenous immunoglobulin; MVI, microvascular inflammation.
Values are expressed as mean ± SD (minimum value; maximum value).

macrophage gene *C5AR1* (complement C5a receptor 1, $P = 3.4E{-}07$, $q = 2.6E{-}04$, logarithm of fold change [Log2FC] = 0.618), the macrophage surface marker *CD163* ($P = 0.0012$, $q = 0.046$, Log2FC = 0.884), and genes related to endothelial processes such as *ACKR1* ($P = 5.6E{-}05$, $q = 0.011$, Log2FC = 0.902), *CDH13* (cadherin 13, $P = 4.6E{-}04$, $q =$

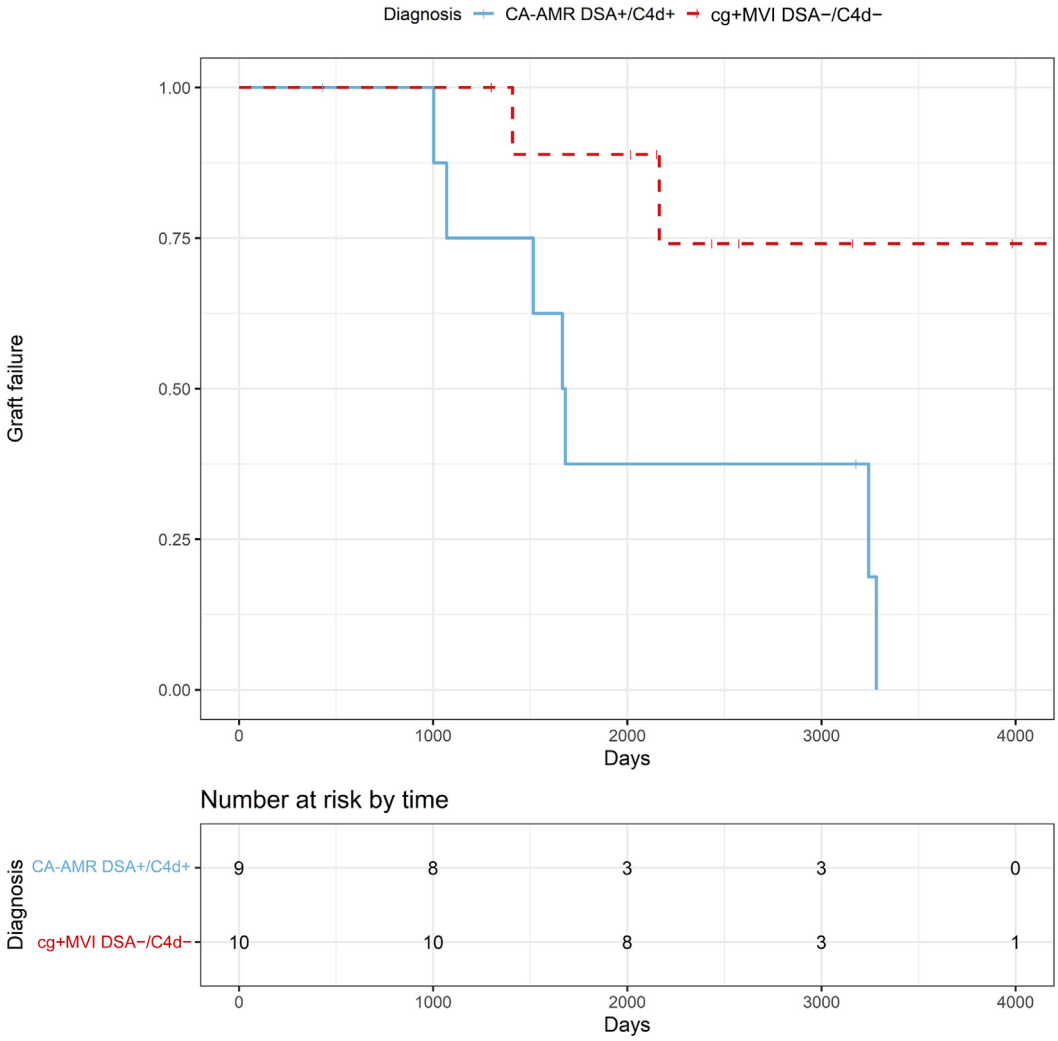

Figure 1 | Kaplan-Meier graft-survival curve for samples diagnosed with cg+MVI DSA$^-$/C4d$^-$ compared with samples diagnosed with CA-AMR DSA$^+$/C4d$^+$. CA-AMR, chronic-active antibody-mediated rejection; *cg*, Banff glomerular basement membrane double contours lesion score; DSA, circulating donor-specific antibodies; MVI, microvascular inflammation.

Table 2 | Differential gene expression analysis

No.	Target	Log2 fold change	*P* value	*q* value
1	C5AR1	0.619	3.35E−07	0.000258
2	FCER1A	−1.46	1.66E−05	0.00478
3	CD8B	−0.882	1.86E−05	0.00478
4	ACKR1	0.903	5.62E−05	0.0108
5	CD207	−0.845	7.77E−05	0.0120
6	AGR2	−1.34	0.000123	0.0158
7	SLC11A1	0.920	0.000168	0.0162
8	CTNNB1	−0.241	0.000189	0.0162
9	LHX6	0.508	0.000153	0.0162
10	ABCE1	−0.267	0.000213	0.0164
11	LILRB2	0.517	0.000319	0.0223
12	PPIA	−0.230	0.000358	0.0230
13	CMKLR1	0.413	0.000403	0.0239
14	CDH13	0.748	0.000457	0.0251
15	C5	−0.460	0.000724	0.0372
16	IFI6	0.884	0.000787	0.0379
17	CAV1	0.757	0.000916	0.0415
18	CD40LG	−0.704	0.000981	0.0420
19	CD163	0.884	0.00115	0.0465

CA-AMR, chronic-active antibody-mediated rejection; *cg*, Banff glomerular basement membrane double contours lesion score; DSA, circulating donor-specific antibodies. Gene expression level comparison of the 15 most differentially expressed genes between cases diagnosed with CA-AMR DSA$^+$/C4d$^+$ and *cg*+MVI DSA$^-$/C4d$^-$ cases using the Banff-Human Organ Transplant Panel with NanoString nCounter technology sorted by the Benjamini-Hochberg–adjusted *P* value (*q* value). Genes with positive Log2 fold change have higher expression in CA-AMR DSA$^+$/C4d$^+$ cases.

0.025, Log2FC = 0.748), and *CAV1* (caveolin 1, $P = 9.2E{-}04$, $q = 0.042$, Log2FC = 0.757). Nine genes displayed higher expression in samples diagnosed with *cg*+MVI DSA$^-$/C4d$^-$ compared with samples diagnosed with CA-AMR DSA$^+$/C4d$^+$, including the cytotoxic T cell–specific gene *CD8B* ($P = 1.9E{-}05$, $q = 0.0048$, Log2FC = −0.882).

Pathway scoring and cell type profiling. Using *GAGE* and custom-made Banff Human Organ Transplant panel–specific pathways,[22] DSA-, CA-AMR-, AMR-, endothelium-, angiogenesis-, interstitial fibrosis and tubular atrophy-, and extracellular matrix–related pathways were enriched in samples diagnosed with CA-AMR DSA$^+$/C4d$^+$ when compared with samples diagnosed with *cg*+MVI DSA$^-$/C4d$^-$. In the same analysis, the T-cell receptor signaling and B cell–associated transcripts (BAT) pathways were enriched in samples diagnosed with *cg*+MVI DSA$^-$/C4d$^-$ when compared with samples diagnosed with CA-AMR DSA$^+$/C4d$^+$ ($P < 0.05$; $q < 0.05$). The 20 most significant pathways are presented in Supplementary Table S4.

Cell type profiling was performed to compare the gene expression analysis findings with those of the mIF analysis. Samples diagnosed with CA-AMR DSA$^+$/C4d$^+$ showed an increase in pan-endothelial cells ($P = 9.2E{-}07$, $q = 1.7{-}05$) and macrophages ($P = 1.9E{-}04$, $q = 0.0017$) in comparison with samples diagnosed with *cg*+MVI DSA$^-$/C4d$^-$. In the same analysis, samples diagnosed with *cg*+MVI DSA$^-$/C4d$^-$ showed an increase in B cells ($P = 3.2E{-}04$, $q = 0.0031$), T cells ($P = 3.4E{-}04$, $q = 0.0031$), and CD45+ cells ($P = 9.8E{-}04$, $q = 0.0059$) in comparison with samples diagnosed with CA-AMR DSA$^+$/C4d$^+$. The complete results of cell type profiling are presented in Supplementary Table S5.

Principal component analysis. The 15 genes with the lowest *q* values in the differential expression analysis were used to generate a principal component analysis biplot. The principal component analysis biplot (Figure 3) visualizing the relationship between the selected genes indicates that the data tend to cluster into 2 distinctly separate groups with similar expression profiles coherently with our initial case diagnosis.

mIF analysis

To evaluate the infiltrate, 2 mIF staining panels were developed. The tubulointerstitial and glomerular compartments were distinguished from each other with manual annotations. For each group, the total surface of the glomeruli and tubulointerstitial compartments of each biopsy were measured. For the tubulointerstitial compartment, the number of cells for each marker per sample was expressed as the mean of the absolute number of cells per tissue area (mm^2). For the glomerular compartment, the number of cells for each marker per sample was expressed as the mean of the absolute number of cells per glomerulus, estimated as the number of cells per surface of a circle with a diameter of 200 μm (0.0314 mm^2) (Table 3).

An example of a kidney biopsy stained with the CD3/CD8/CD68/CD31/C4d mIF panel (panel 1) is shown in Figure 4a. The biopsies were stained with CD3 (white), CD8 (green), CD68 (aqua), CD31 (red), and C4d (gold) (Figure 4b). A visual summary of the results is presented in Figure 5a and b. One case was excluded from the analysis of the tubulointerstitial compartment as it was a significant outlier. The number of CD3+ cells was significantly higher in the glomeruli of *cg*+MVI DSA$^-$/C4d$^-$ cases when compared with CA-AMR DSA$^+$/C4d$^+$ cases (17.60 ± 11.32 vs. 5.00 ± 4.77/glomerulus, respectively, $P = 0.0075$; Figure 5a). Analysis of CD3+ subtypes revealed that the number of both CD3$^+$/CD8$^+$ and CD3$^+$/CD8$^-$ cells was significantly higher in the glomeruli of *cg*+MVI DSA$^-$/C4d$^-$ cases compared with CA-AMR DSA$^+$/C4d$^+$ cases (8.50 ± 6.00 vs. 2.22 ± 2.44/glomerulus, respectively, $P = 0.013$; 9.20 ± 6.44 vs. 2.44 ± 2.51/glomerulus, respectively, $P = 0.010$; Figure 5a).

An example of a kidney biopsy stained with the CD68/CD163/CD16/CD14/CD56 mIF panel (panel 2) is shown in Figure 6a. The biopsies were stained with CD14 (yellow), CD16 (green), CD68 (aqua), CD56 (white), and CD163 (red) (Figure 6b). A visual summary of the results is presented in Figure 5c and d. The number of interstitial CD16$^+$CD56$^+$ positive cells was significantly higher in cases with CA-AMR DSA$^+$/C4d$^+$ compared with cases with *cg*+MVI DSA$^-$/C4d$^-$ (207.56 ± 191.58/mm^2 vs. 59.00 ± 38.49/mm^2, respectively, $P = 0.035$; Figure 5d). The number of CD163$^+$ positive cells was higher, without reaching statistical significance, in the interstitial compartment of the CA-AMR DSA$^+$/C4d$^+$ cases when compared with *cg*+MVI DSA$^-$/C4d$^-$ (788.67 ± 548.22/mm^2 vs. 309.80 ± 249.95/mm^2, respectively, $P = 0.065$; Figure 5d).

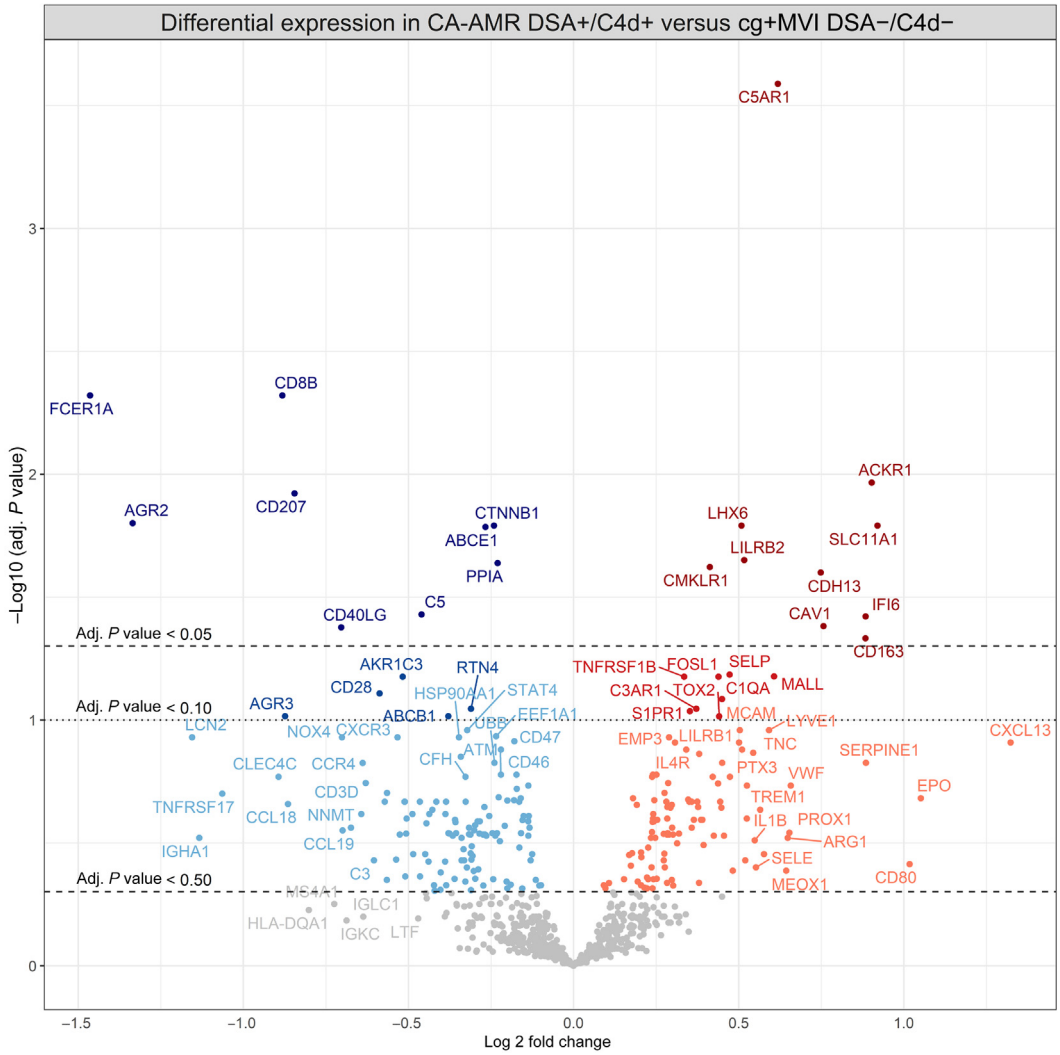

Figure 2 | Gene expression volcano plot representing the gene expression profile of the CA-AMR DSA$^+$/C4d$^+$ study group compared with the *cg*+MVI DSA$^-$/C4d$^-$ study group. The *x*-axis corresponds to the fold change (Log2 transformed) and the *y*-axis represents the *P* value (−Log10). The horizontal dashed lines represent the adjusted (adj.) *P* value (*q* value) thresholds. CA-AMR, chronic-active antibody-mediated rejection; *cg*, Banff glomerular basement membrane double contours lesion score; DSA, circulating donor-specific antibodies; MVI, microvascular inflammation.

Sirius Red staining

Sirius Red staining was performed to investigate the amount of interstitial fibrosis (Figure 7). The area percentage of Sirius Red staining in cortical tissue was not significantly different between the cases with CA-AMR DSA$^+$/C4d$^+$ and *cg*+MVI DSA$^-$/C4d$^-$ (16.6% ± 18.3% vs. 17.4% ± 12.1%, respectively; $P = 0.91$).

DISCUSSION

This multicenter intercontinental study included a well-defined cohort of patients to shed light on the pathogenesis of TG in the presence of MVI and in the absence of both DSAs and C4d staining of ptcs. We compared the transcriptomic profile of for-cause KTx biopsies classified as CA-AMR DSA$^+$/C4d$^+$ with those classified as *cg*+MVI DSA$^-$/C4d$^-$ and successfully confirmed our results on a subset of the cohort through orthogonal analyses using a novel mIF protein analysis methodology. To do so, we have used 2 novel state-of-the-art technologies, namely NanoString nCounter transcriptomic analysis and two 5-plex mIF panels. We show that cases diagnosed with CA-AMR DSA$^+$/C4d$^+$ had an environment characterized by an increased presence and activity of innate immune cells, such as macrophages, neutrophils, natural killer cells, and other monocytes. As expected, the CA-AMR DSA$^+$/C4d$^+$ environment was also characterized by higher expression of AMR-, angiogenesis-, and complement-related genes (e.g., *C5AR1*). In contrast to current belief, KTx biopsies diagnosed with *cg*+MVI DSA$^-$/C4d$^-$ had a higher abundance of T cells and T-cell activation.

In CA-AMR, the classical pathway of complement is activated by DSAs binding to HLA on the endothelial cells of the allograft.[29] For this reason, the elevated expression of complement-related genes such as *C5AR1* in the CA-AMR DSA$^+$/C4d$^+$ group can be explained by the occurrence of a

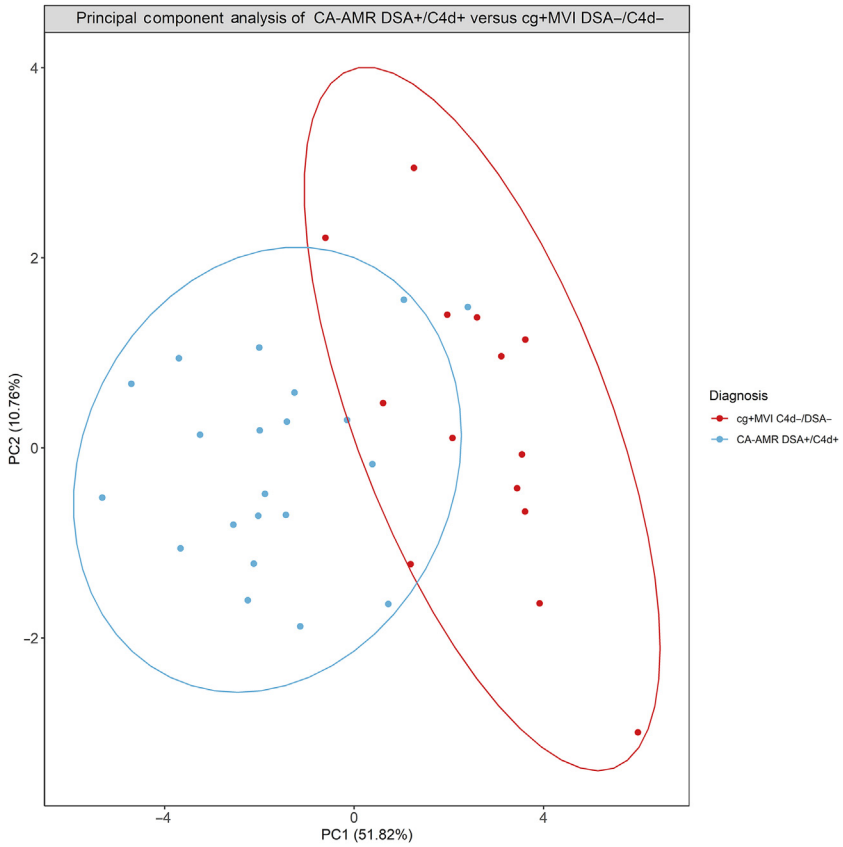

Figure 3 | Principal component (PC) analysis plot representing the 15 differentially expressed genes with the lowest *q* values. CA-AMR, chronic-active antibody-mediated rejection; *cg*, Banff glomerular basement membrane double contours lesion score; DSA, circulating donor-specific antibodies; MVI, microvascular inflammation.

more antibody-mediated process compared with *cg*+MVI DSA$^-$/C4d$^-$. In a 2010 study by Li *et al.*,[30] C5aR was shown to be important for a full adaptive immune response and to mediate KTx rejection. In addition, *C5aR* expression increased in human KTxs with acute rejection compared with normal kidney tissue, and superior long-term allograft

Table 3 | mIF analysis results overview

	Glomeruli (counts/glomerulus)					Interstitium (counts/mm^2)				
	CA-AMR DSA$^+$/C4d$^+$		*cg*+MVI DSA$^-$/C4d$^-$			CA-AMR DSA$^+$/C4d$^+$		*cg*+MVI DSA$^-$/C4d$^-$		
Cell type	Mean	SD	Mean	SD	*P* value	Mean	SD	Mean	SD	*P* value
Panel 1										
CD3	5.00	4.77	17.60	11.32	0.007[a]	371.25	159.67	330.22	187.30	0.738
CD3$^+$/CD8$^+$	2.22	2.44	8.50	6.00	0.013[a]	135.25	55.58	160.11	156.69	0.661
CD3$^+$/CD8$^-$	2.44	2.51	9.20	6.44	0.010[a]	236.00	108.69	217.70	137.74	0.900
CD31	143.75	40.14	157.40	62.07	0.599	831.75	541.01	530.90	348.20	0.294
C4d	73.63	60.07	38.20	62.14	0.021[a]	34.17	26.07	17.30	20.11	0.027[a]
CD68	37.89	34.50	51.01	20.39	0.453	787.80	694.93	750.10	427.40	0.117
Panel 2										
CD14	21.22	26.89	20.30	26.75	0.720	751.67	572.51	501.30	543.56	0.243
CD16	10.89	7.25	9.40	10.01	0.356	453.56	268.09	262.40	175.27	0.182
CD14$^+$CD16$^+$	5.00	6.38	5.50	8.89	0.720	253.89	171.64	148.70	184.85	0.113
CD68	18.56	26.38	15.00	7.79	0.400	335.44	451.58	120.30	94.12	0.158
CD163	27.67	22.81	18.30	13.76	0.121	788.67	548.22	309.80	249.95	0.065
CD163$^+$68$^+$	11.33	14.85	3.40	1.90	0.243	338.22	264.88	122.00	62.31	0.156
CD16$^+$56$^+$	4.78	4.79	1.90	1.91	0.182	207.56	191.58	59.00	38.49	0.035[a]

CA-AMR, chronic-active antibody-mediated rejection; *cg*, Banff glomerular basement membrane double contours lesion score; DSA, circulating donor-specific antibodies; mIF, multiplex immunofluoresence; MVI, microvascular inflammation.
[a]$P < 0.05$.

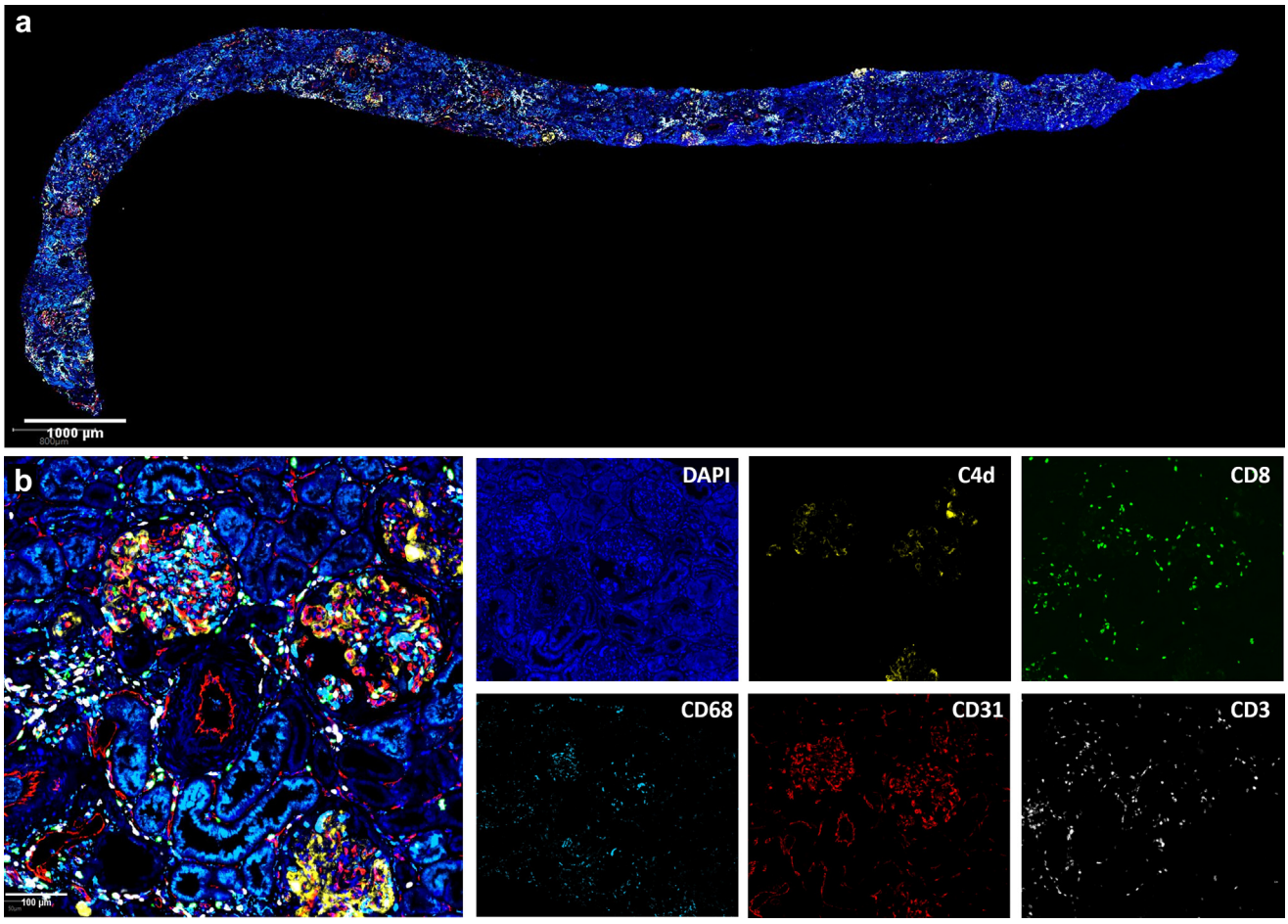

Figure 4| Multiplex immunofluorescent staining of panel 1 on kidney transplant biopsy section. (**a**) Overview of formalin-fixed paraffin-embedded kidney biopsy labeled with CD3 (white), CD8 (green), CD68 (aqua), CD31 (red), and C4d (gold), and stained with DAP; (**b**) detail displaying how the tubulointerstitial part could be distinguished from the glomerular with annotations (red circle). Original magnification ×200. DAPI, 4′,6-diamidino-2-phenylindole. To optimize viewing of this image, please see the online version of this article at www.kidney-international.org.

survival and reduced infiltration of macrophages were shown in mice KTx models with deficiency or inhibition of *C5aR*.[31] Our finding that KTx biopsies with *cg*+MVI DSA$^-$/C4d$^-$ have significantly lower expression levels of *C5AR1* and lower macrophage presence and activity compared with KTx biopsies with CA-AMR DSA$^+$/C4d$^+$ is consistent with literature.

Cases diagnosed as CA-AMR DSA$^+$/C4d$^+$ have an environment characterized by a greater degree of innate immune activity. Literature shows that the treatment of endothelial cells with HLA class I antibodies can lead to the recruitment of leukocytes such as neutrophils and macrophages[32,33] and, moreover, fragments generated through complement activation could activate the same cell types.[34] Cell-type quantification through mIF revealed a higher amount of CD163$^+$ (macrophages) and CD16$^+$CD56$^+$ (natural killer cells) cells in the tubulointerstitial compartment of samples diagnosed as CA-AMR DSA$^+$/C4d$^+$ compared with samples diagnosed with *cg*+MVI DSA$^-$/C4d$^-$. These results confirmed the increased macrophage cell type score and mRNA expression levels of the macrophage-specific markers *CD163* and *C5AR1* found in cases with CA-AMR DSA$^+$/C4d$^+$.

Angiogenesis and fibrosis are of pathologic significance in chronic inflammatory diseases such as chronic allograft rejection. The presence of HLA-DSAs and the dominant mononuclear cell infiltrate characterizing CA-AMR DSA$^+$/C4d$^+$ samples could sustain these processes. Literature shows how the persistent local expression of angiogenesis factors from macrophages and mononuclear cells could assist in sustaining the angiogenesis response[35–38] and, in contrast with antecedent findings,[39] HLA-DSAs could be a major cause of accelerated allograft fibrosis.[40] The elevated angiogenesis, endothelium, endothelial DSA-selective transcripts, extracellular matrix, and interstitial fibrosis and tubular atrophy pathway scores in cases with CA-AMR DSA$^+$/C4d$^+$, in addition to the elevated macrophage cell type scores and quantification and the increased expression of *C5AR1*, are therefore in accordance with recent existing literature. However, histomorphologic assessment and area percentage of fibrosis (Sirius Red staining) did not differ between the 2

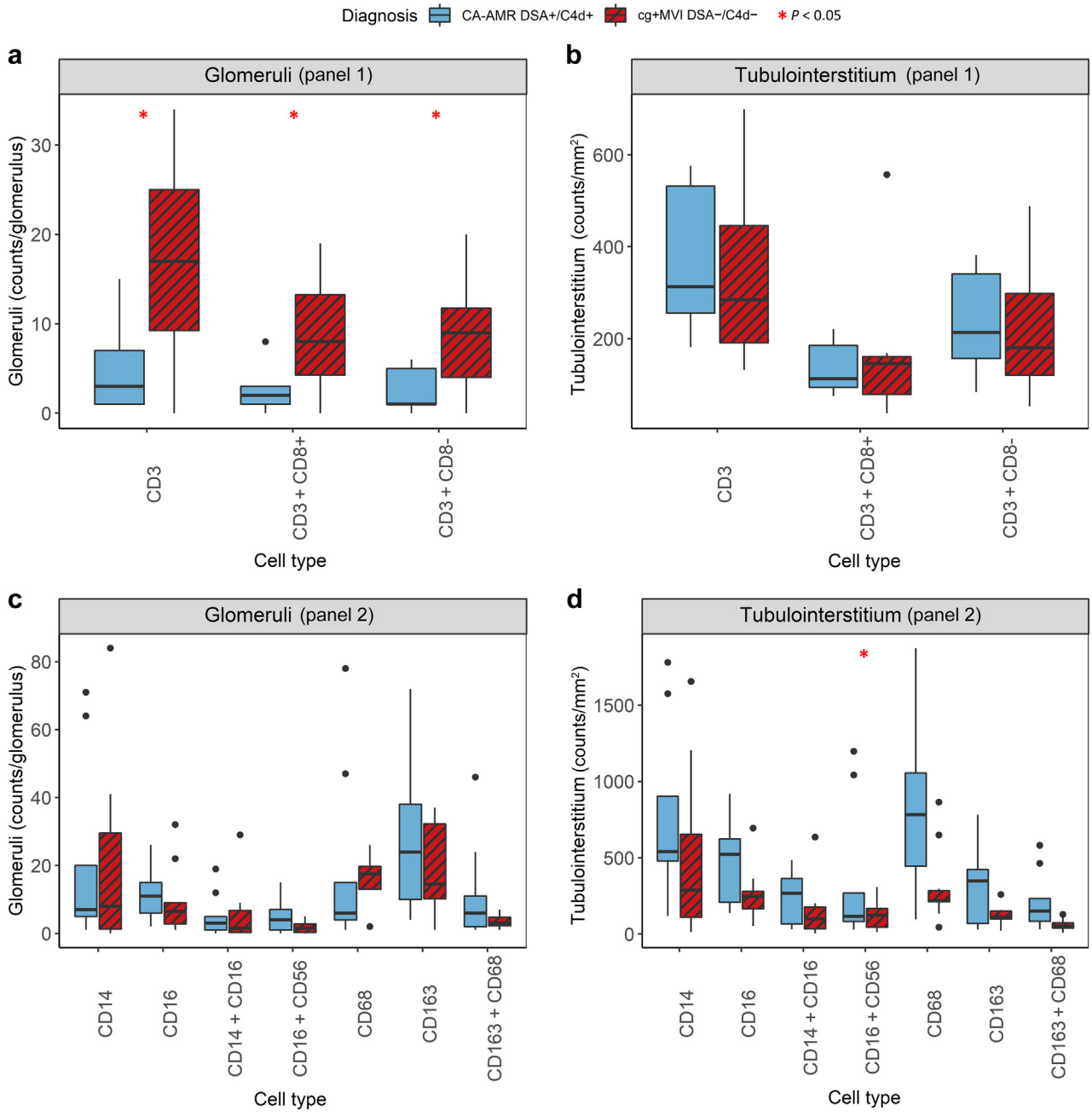

Figure 5 | Immune and inflammatory cell repertoires of samples diagnosed with *cg*+MVI DSA$^-$/C4d$^-$ compared with samples diagnosed with CA-AMR DSA$^+$/C4d$^+$. Results of multiplex immunofluorescent staining followed by QuPath analysis. (**a**) Panel 1—glomeruli; (**b**) panel 1—tubulointerstitium; (**c**) panel 2—glomeruli; and (**d**) panel 2—tubulointerstitium. CA-AMR, chronic-active antibody-mediated rejection; *cg*, Banff glomerular basement membrane double contours lesion score; DSA, circulating donor-specific antibodies; MVI, microvascular inflammation.

study groups. This is although coherent with existing literature showing how the Banff *cg*– score, also not different between our study groups, is not correlated with the incidence and severity of interstitial fibrosis. Our findings might also suggest that a more severe and persistent chronic inflammatory state affects patients diagnosed with CA-AMR DSA$^+$/C4d$^+$ in comparison with those diagnosed with *cg*+MVI DSA$^-$/C4d$^-$, but further research is needed to better understand the relationship between these processes and the DSA/C4d status.

During the last Banff meeting in September 2022 in Banff, Canada, discussions focused on how not all MVIs could be attributed to an antibody-mediated response. In our study, samples diagnosed with *cg*+MVI DSA$^-$/C4d$^-$ showed a significantly higher abundance of glomerular CD3$^+$ cells (pan T cells), CD3$^+$CD8$^+$ cells (cytotoxic T cells), and CD3$^+$CD8$^-$

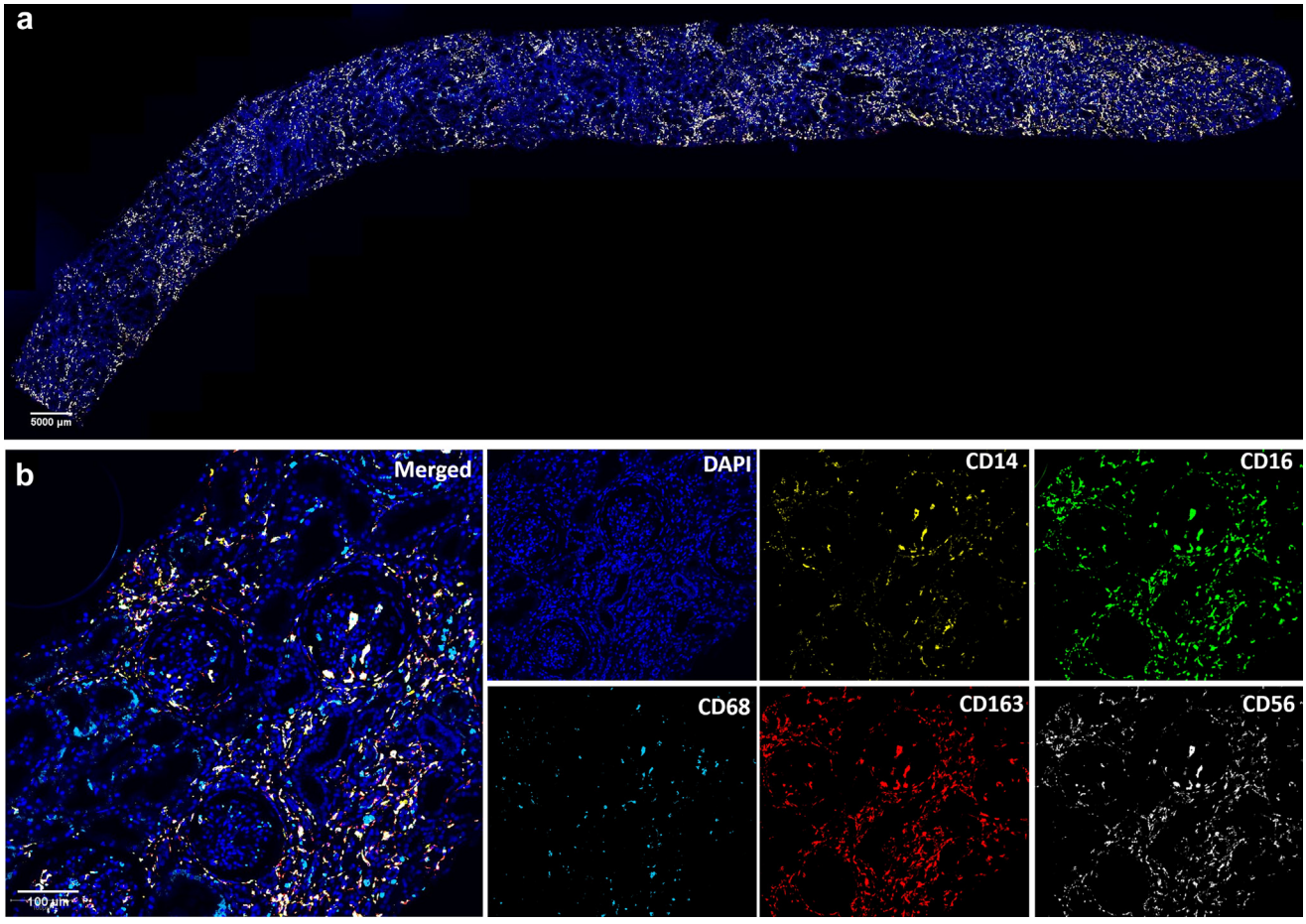

Figure 6| Multiplex immunofluorescent staining of panel 2 on kidney transplant biopsy section. (**a**) Overview of formalin-fixed paraffin-embedded kidney biopsy labeled with CD14 (gold), CD16 (green), CD68 (aqua), CD163 (red), and CD56 (white), and stained with DAP; (**b**) detail displaying how the tubulointerstitial part could be distinguished from the glomerular with annotations (red circle). Original magnification ×200. To optimize viewing of this image, please see the online version of this article at www.kidney-international.org.

cells (noncytotoxic T cells), confirming the higher T cells cell type score and higher mRNA expression levels of the cytotoxic T cell–specific gene *CD8B*. This is in accordance with previous findings showing higher T-cell presence in MVI DSA$^-$/C4d$^-$ samples when compared with samples diagnosed with AMR DSA$^+$/C4d$^+$.[41] This increase in T cells is not associated with the extent of glomerulitis as assessed by the Banff "*g*" individual lesion score as that was comparable between the 2 groups. Existing literature supports a role of T cell–mediated activity in the development of transplant glomerulitis (and subsequent increase in *cg*– score) in the absence of DSAs.[42,43] The same activity could lead to chronic endothelial cell activation, as seen in the larger arteries of patients diagnosed with T cell–mediated rejection, resulting in chronic vasculopathy. Thus, samples fulfilling the histologic criteria for the CA-AMR diagnosis but lacking circulating DSAs and C4d staining of ptcs seem to be characterized by greater T-cell activity, a process that greatly distinguishes them from samples diagnosed with CA-AMR. Our results cast doubt on the comparability of *cg*+MVI DSA$^-$/C4d$^-$ with the Banff diagnostic category of CA-AMR, with potential therapeutic implications.

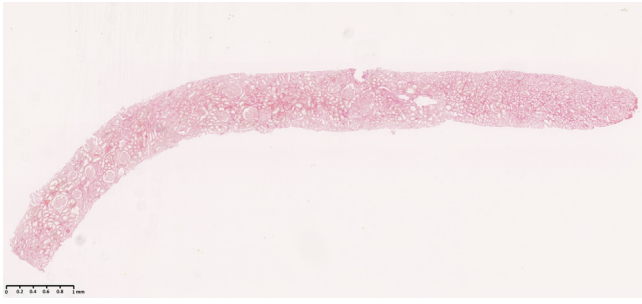

Figure 7| Sirius Red staining in kidney biopsy. Slide scanned with the Hamamatsu NanoZoomer; original magnification ×40. Vibrant red represents fibrosis. To optimize viewing of this image, please see the online version of this article at www.kidney-international.org.

Cases with CA-ABMR DSA$^+$/C4d$^+$ were characterized by different environments and pathological processes that could explain their inferior graft survival when compared with cases with *cg*+MVI DSA$^-$/C4d$^-$, as this is also coherent with

existing literature reporting worse outcomes for KTxs characterized by increased interstitial fibrosis and tubular atrophy and extracellular matrix deposition.[44–46] Moreover, therapeutical strategy could have played a major role in the superior outcome of cases with *cg*+MVI DSA$^-$/C4d$^-$, as all Erasmus MC cases received equal treatment, namely single course of i.v. Igs and pulse i.v. methylprednisolone.[47] Our findings have put forward a more T cell–associated phenotype; however, this does not exclude the possibility that these 2 phenotypes could represent 2 different degrees of activity of AMR. Further research is needed to better understand to which extent the pathogenesis of these processes differ; the new Banff Activity and Chronicity Indices Working Group will help in elucidating this.[18]

Our study has several limitations, including its retrospective nature limiting the strength of its findings and the small population size. Considering the aim of this study and the high intraobserver and interobserver variabilities that characterize histomorphologic graft evaluation, we deemed the selection of appropriate high-quality samples more important than the sample size, and the 36 samples were strictly selected to avoid possible confounding variables. Moreover, our mIF orthogonal analysis confirmed the results of our gene expression analysis on a different data type.

Our findings support the existence of 2 distinguished chronic-active transplant rejection subtypes, namely Banff category 2 CA-AMR DSA$^+$/C4d$^+$ and the ambiguous *cg*+MVI DSA$^-$/C4d$^-$, characterized by higher abundance of infiltrating T cells and lower complement and innate immune activity. A more accurate subclassification could allow for a more tailored therapeutic approach to further increase transplant outcome and patient quality of life, particularly given the higher T-cell abundance and activity in cases with *cg*+MVI DSA$^-$/C4d$^-$.

In conclusion, *cg*+MVI DSA$^-$/C4d$^-$ is currently not described as a diagnosis in the Banff Classification of Allograft Pathology. Our results suggest the presence of a more T-cell dominant phenotype in cases with *cg*+MVI DSA$^-$/C4d$^-$ compared with CA-AMR DSA$^+$/C4d$^+$, putting forward the possibility that these are not a variant of AMR and therefore might require a different therapeutical management. More research is needed to confirm and expand our findings to fully understand the pathogenesis of these 2 subtypes of chronic-active transplant rejection and to assess potential differences in therapy response and subsequent transplant outcome.

DISCLOSURE

The authors declare no competing interests directly related to this work. The authors however disclose unrelated funding, honorariums, and ownership as follows: RK has grants from Travere Therapeutics, Galapagos, Chugai, and Novo Nordisk, and is a consultant for Bayer, Pfizer, Novo Nordisk, and Gruenenthal. MvB was employed by company Omnigen BV. DAH has received lecture fees and consulting fees from Astellas Pharma, AstraZeneca, Chiesi Pharma, Medincell, Novartis Pharma, Sangamo Therapeutics, and Vifor Pharma; and grant support from Astellas Pharma, Bristol-Myers Squibb, and Chiesi Pharma (paid to his institution); he does not have employment or stock ownership at any of these companies, nor does he have patents or patent applications. MCC-vG received grant support from Astellas Pharma (paid to her institution). All other authors declared no competing interests.

DATA STATEMENT

The gene expression data supporting the findings of this study are openly available in the Gene Expression Omnibus repository with accession number GSE242984. The code used in the analyses is available on GitHub at https://github.com/PapXis/CA-AMR_Study_Analysis.

SUPPLEMENTARY MATERIAL

Supplementary File (Word)

Supplementary Table S1. Overview of the multiplex immunofluorescence staining panels.

Supplementary Table S2. Histologic evaluation according to the Banff Classification 2019 update.

Supplementary Table S4. Pathway scoring analysis results.

Supplementary Table S5. Cell-type analysis results.

Supplementary Methods.

Supplementary References.

Supplementary File (Excel)

Supplementary Table S3. Full gene expression analysis results.

REFERENCES

1. Sellarés J, de Freitas DG, Mengel M, et al. Understanding the causes of kidney transplant failure: the dominant role of antibody-mediated rejection and nonadherence. *Am J Transplant*. 2012;12:388–399.
2. Naesens M, Kuypers DRJ, De Vusser K, et al. The histology of kidney transplant failure: a long-term follow-up study. *Transplantation*. 2014;98:427–435.
3. Pouliquen E, Koenig A, Chen CC, et al. Recent advances in renal transplantation: antibody-mediated rejection takes center stage. *F1000Prime Rep*. 2015;7:51.
4. Valenzuela NM, Reed EF. Antibody-mediated rejection across solid organ transplants: manifestations, mechanisms, and therapies. *J Clin Invest*. 2017;127:2492–2504.
5. Loupy A, Haas M, Roufosse C, et al. The Banff 2019 Kidney Meeting Report (I): updates on and clarification of criteria for T cell- and antibody-mediated rejection. *Am J Transplant*. 2020;20:2318–2331.
6. Haas M. The revised (2013) Banff classification for antibody-mediated rejection of renal allografts: update, difficulties, and future considerations. *Am J Transplant*. 2016;16:1352–1357.
7. Lucia M, Luque S, Crespo E, et al. Preformed circulating HLA-specific memory B cells predict high risk of humoral rejection in kidney transplantation. *Kidney Int*. 2015;88:874–887.
8. Snanoudj R, Claas FH, Heidt S, et al. Restricted specificity of peripheral alloreactive memory B cells in HLA-sensitized patients awaiting a kidney transplant. *Kidney Int*. 2015;87:1230–1240.
9. Michielsen LA, van Zuilen AD, Krebber MM, et al. Clinical value of non-HLA antibodies in kidney transplantation: still an enigma? *Transplant Rev (Orlando)*. 2016;30:195–202.
10. Dragun D, Catar R, Philippe A. Non-HLA antibodies against endothelial targets bridging allo- and autoimmunity. *Kidney Int*. 2016;90:280–288.
11. Sigdel TK, Li L, Tran TQ, et al. Non-HLA antibodies to immunogenic epitopes predict the evolution of chronic renal allograft injury. *J Am Soc Nephrol*. 2012;23:750–763.
12. Pineda S, Sigdel TK, Chen J, et al. Corrigendum: novel non-histocompatibility antigen mismatched variants improve the ability to predict antibody-mediated rejection risk in kidney transplant. *Front Immunol*. 2018;9:107.
13. Akalin E, Dinavahi R, Dikman S, et al. Transplant glomerulopathy may occur in the absence of donor-specific antibody and C4d staining. *Clin J Am Soc Nephrol*. 2007;2:1261–1267.
14. Cohen D, Colvin RB, Daha MR, et al. Pros and cons for C4d as a biomarker. *Kidney Int*. 2012;81:628–639.

15. Gloor JM, Sethi S, Stegall MD, et al. Transplant glomerulopathy: subclinical incidence and association with alloantibody. *Am J Transplant*. 2007;7:2124–2132.
16. Becker LE, Morath C, Suesal C. Immune mechanisms of acute and chronic rejection. *Clin Biochem*. 2016;49:320–323.
17. Hidalgo LG, Sis B, Sellares J, et al. NK cell transcripts and NK cells in kidney biopsies from patients with donor-specific antibodies: evidence for NK cell involvement in antibody-mediated rejection. *Am J Transplant*. 2010;10:1812–1822.
18. Naesens M, Roufosse C, Colvin RB, et al. The Banff 2022 Kidney Meeting Report: re-appraisal of microvascular inflammation and the role of biopsy-based transcript diagnostics. Published online October 28 *Am J Transplant*. 2023. https://doi.org/10.1016/j.ajt.2023.10.016
19. Callemeyn J, Lerut E, de Loor H, et al. Transcriptional changes in kidney allografts with histology of antibody-mediated rejection without anti-HLA donor-specific antibodies. *J Am Soc Nephrol*. 2020;31:2168–2183.
20. Haas M. Transplant glomerulopathy: it's not always about chronic rejection. *Kidney Int*. 2011;80:801–803.
21. Baid-Agrawal S, Farris AB, Pascual M, et al. Overlapping pathways to transplant glomerulopathy: chronic humoral rejection, hepatitis C infection, and thrombotic microangiopathy. *Kidney Int*. 2011;80:879–885.
22. Rosales IA, Mahowald GK, Tomaszewski K, et al. Banff human organ transplant transcripts correlate with renal allograft pathology and outcome: importance of capillaritis and subpathologic rejection. *J Am Soc Nephrol*. 2022;33:2306–2319.
23. Mengel M, Loupy A, Haas M, et al. Banff 2019 Meeting Report: molecular diagnostics in solid organ transplantation-consensus for the Banff Human Organ Transplant (B-HOT) gene panel and open source multicenter validation. *Am J Transplant*. 2020;20:2305–2317.
24. Bankhead P, Loughrey MB, Fernández JA, et al. QuPath: open source software for digital pathology image analysis. *Sci Rep*. 2017;7:16878.
25. Bhattacharya A, Hamilton AM, Furberg H, et al. An approach for normalization and quality control for NanoString RNA expression data. *Brief Bioinform*. 2021;22:bbaa163.
26. Love MI, Huber W, Anders S. Moderated estimation of fold change and dispersion for RNA-seq data with DESeq2. *Genome Biol*. 2014;15:550.
27. Haynes W. Benjamini–Hochberg method. In: Dubitzky W, Wolkenhauer O, Cho K-H, Yokota H, eds. *Encyclopedia of Systems Biology*. Springer; 2013:78.
28. Luo W, Friedman MS, Shedden K, et al. GAGE: generally applicable gene set enrichment for pathway analysis. *BMC Bioinformatics*. 2009;10:161.
29. Stites E, Le Quintrec M, Thurman JM. The complement system and antibody-mediated transplant rejection. *J Immunol*. 2015;195:5525–5531.
30. Li Q, Peng Q, Xing G, et al. Deficiency of C5aR prolongs renal allograft survival. *J Am Soc Nephrol*. 2010;21:1344–1353.
31. Gueler F, Rong S, Gwinner W, et al. Complement 5a receptor inhibition improves renal allograft survival. *J Am Soc Nephrol*. 2008;19:2302–2312.
32. Zhang X, Valenzuela NM, Reed EF. HLA class I antibody-mediated endothelial and smooth muscle cell activation. *Curr Opin Organ Transplant*. 2012;17:446–451.
33. Lee C-Y, Lotfi-Emran S, Erdinc M, et al. The involvement of FcR mechanisms in antibody-mediated rejection. *Transplantation*. 2007;84:1324–1334.
34. Grafals M, Thurman JM. The role of complement in organ transplantation. *Front Immunol*. 2019;10:2380.
35. Reinders MEJ, Rabelink TJ, Briscoe DM. Angiogenesis and endothelial cell repair in renal disease and allograft rejection. *J Am Soc Nephrol*. 2006;17:932–942.
36. Reinders MEJ, Briscoe DM. Angiogenesis and allograft rejection. *Graft*. 2002;5:96–101.
37. Ramirez-Pedraza M, Fernández M. Interplay between macrophages and angiogenesis: a double-edged sword in liver disease. *Front Immunol*. 2019;10:2882.
38. Polverini PJ. Role of the macrophage in angiogenesis-dependent diseases. In: Goldberg ID, Rosen EM, eds. *Regulation of Angiogenesis*. Birkhäuser; 1997:11–28.
39. Webster AC, Craig JC, Simpson JM, et al. Identifying high risk groups and quantifying absolute risk of cancer after kidney transplantation: a cohort study of 15,183 recipients. *Am J Transplant*. 2007;7:2140–2151.
40. Gosset C, Viglietti D, Rabant M, et al. Circulating donor-specific anti-HLA antibodies are a major factor in premature and accelerated allograft fibrosis. *Kidney Int*. 2017;92:729–742.
41. Buxeda A, Llinàs-Mallol L, Gimeno J, et al. Microvascular inflammation in the absence of human leukocyte antigen-donor-specific antibody and C4d: an orphan category in Banff classification with cytotoxic T and natural killer cell infiltration. *Am J Transplant*. 2023;23:464–474.
42. Senev A, Van Loon E, Lerut E, et al. Risk factors, histopathological features, and graft outcome of transplant glomerulopathy in the absence of donor-specific HLA antibodies. *Kidney Int*. 2021;100:401–414.
43. Coemans M, Senev A, Van Loon E, et al. The evolution of histological changes suggestive of antibody-mediated injury, in the presence and absence of donor-specific anti-HLA antibodies. *Transpl Int*. 2021;34:1824–1836.
44. Mannon RB, Matas AJ, Grande J, et al. Inflammation in areas of tubular atrophy in kidney allograft biopsies: a potent predictor of allograft failure. *Am J Transplant*. 2010;10:2066–2073.
45. Vuiblet V, Fere M, Gobinet C, et al. Renal graft fibrosis and inflammation quantification by an automated Fourier–transform infrared imaging technique. *J Am Soc Nephrol*. 2016;27:2382–2391.
46. Modena BD, Kurian SM, Gaber LW, et al. Gene expression in biopsies of acute rejection and interstitial fibrosis/tubular atrophy reveals highly shared mechanisms that correlate with worse long-term outcomes. *Am J Transplant*. 2016;16:1982–1998.
47. Sablik KA, Clahsen-van Groningen MC, Looman CWN, et al. Treatment with intravenous immunoglobulins and methylprednisolone may significantly decrease loss of renal function in chronic-active antibody-mediated rejection. *BMC Nephrol*. 2019;20:218.